



Computational investigation of peptidomimetics as potential inhibitors of SARS-CoV-2 spike protein

Mayar Tarek Ibrahim and Peng Tao 

Department of Chemistry, Center for Research Computing, Center for Drug Discovery, Design, and Delivery (CD4), Southern Methodist University, Dallas, TX, USA

Communicated by Ramaswamy H. Sarma

ABSTRACT

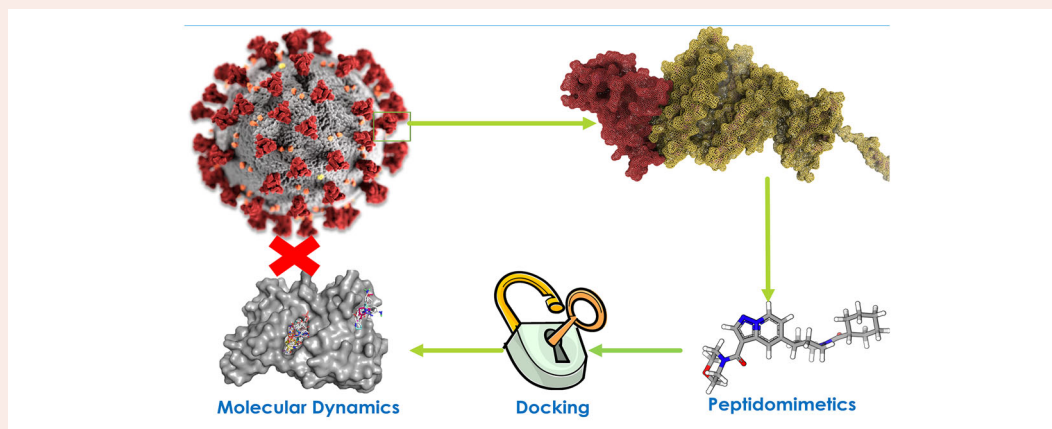
Several variants of the severe acute respiratory syndrome coronavirus 2 (SARS-CoV-2) were observed since the outbreak of the global pandemic at the end of 2019. The trimeric spike glycoprotein of the SARS-CoV-2 virus is crucial for the viral access to the host cell by interacting with the human angiotensin converting enzyme 2 (ACE2). Most of the mutations take place in the receptor-binding domain (RBD) of the S1 subunit of the trimeric spike glycoprotein. In this work, we targeted both S1 and S2 subunits of the spike protein in the wild type (WT) and the Omicron variant guided by the interaction of the neutralizing monoclonal antibodies. Virtual screening of two different peptidomimetics databases, ChEMBL and ChemDiv databases, was carried out against both S1 and S2 subunits. The use of these two databases provided diversity and enhanced the chance of finding protein-protein interaction inhibitors (PPIIs). Multi-layered filtration, based on physicochemical properties and docking scores, of nearly 114,000 compounds found in the ChEMBL database and nearly 14,000 compounds in the ChemDiv database was employed. Four peptidomimetics compounds were effective against both the WT and the Omicron S1 subunit with the minimum binding free energy of -25 kcal/mol. Five peptidomimetics compounds were effective against the S2 subunit with the minimum binding free energy of -19 kcal/mol. The dynamical cross-correlation matrix insinuated that the mutations of the RBD in the Omicron variant of the SARS-CoV-2 virus altered the correlated conformational motion of the different regions of the protein.

ARTICLE HISTORY

Received 1 June 2022
Accepted 18 August 2022

KEYWORDS



SARS-CoV-2 spike protein;
Omicron variant;
peptidomimetics; MM/GBSA;
dynamical cross-
correlation matrix




1. Introduction

Severe Acute Respiratory Syndrome Coronavirus 2 (SARS-CoV-2) belongs to the Coronaviruses (CoVs) subfamily, which are characterized by the presence of spikes on their surface (Cui et al., 2019; Kim et al., 2022; Zhu et al., 2020). CoVs group was the cause behind several outbreaks: Severe Acute Respiratory Syndrome Coronavirus (SARS-CoV), Middle

Eastern Respiratory Syndrome Coronavirus (MERS-CoV), and recently SARS-CoV-2 (Knipe, 2013; Lu et al., 2015; Su et al., 2016). Despite the development of vaccines, the global pandemic is still an issue of concern due to the emerging variants of SARS-CoV-2. The emerging variants are associated with enhanced transferability and a higher infection rate due to the evasion of the immune system (Campbell et al., 2021;

CONTACT Peng Tao  ptao@smu.edu  Department of Chemistry, Center for Research Computing, Center for Drug Discovery, Design, and Delivery (CD4), Southern Methodist University, Dallas, TX, USA

 Supplemental data for this article can be accessed online at <https://doi.org/10.1080/07391102.2022.2116601>.

© 2022 Informa UK Limited, trading as Taylor & Francis Group

Hoffmann et al., 2021). These variants include B.1.1.7 (SARS-CoV-2 α), B.1.351 (β), P.1 (γ), B.1.617.2 (δ), and B.1.1.529 (SARS-CoV-2 Omicron) (Colmenares-Mejía et al., 2021; Du, 2022; Liu et al., 2021; Zhou et al., 2021). The observed mutations in the emerging variants of SARS-CoV-2 are mostly located in the receptor-binding domain (RBD) of the S1 subunit of the spike glycoprotein.

The trimeric spike glycoprotein is a class I fusion protein present on the surface of the SARS-CoV-2 virus facilitating access to the host cell (Li, 2016; Walls et al., 2020). The S protein consists of two subunits: S1 and S2 (Zamzami et al., 2022). The RBD of the S1 subunit recognizes and interacts with the human angiotensin converting enzyme 2 (ACE2) protein (Rabbani & Ahn, 2021). S2 subunit is essential for the fusion of the host and the viral membranes (Hoffmann et al., 2020; Li, 2015). As the spike protein has a crucial role in the life cycle of the virus, the developed mRNA vaccines are based on immunogens of the S protein (Baden, 2020; Polack et al., 2020; Voysey et al., 2021).

Despite the discovery of peptides effective in inhibiting the RBD of the spike protein of the SARS-CoV-2 virus (Rabbani et al., 2021), peptides are subject to high proteolysis and poor oral absorption resulting in low bioavailability. On the other hand, peptidomimetics have better bioavailability, duration of action, selectivity, and potency (Cowell et al., 2004; Vagner et al., 2008). Peptidomimetics are designed to interact with the biological targets and to produce a similar biological effect to natural peptides or proteins. In other words, peptidomimetics are compounds that resemble natural peptides or proteins but with better physicochemical activity. Peptidomimetics were found to be effective in a wide range of studies. For example, peptidomimetics were used as antimicrobial agents mimicking the antimicrobial peptides but with improved stability (Molchanova et al., 2017), gastrointestinal prokinetic agents with enhanced oral bioavailability (Dale et al., 2011), and antimalarial agents with improved in-vivo activity (Patrick, 2020). In addition, peptidomimetics were used to mimic the specificity and the affinity of the antibody binding and to produce the same biological activity (Sachdeva et al., 2019). Therefore, using peptidomimetics to mimic the interactions of the monoclonal neutralizing antibodies to inhibit both S1 and S2 subunits of SARS-CoV-2 spike protein is promising.

Several studies have been carried out so far targeting the SARS-CoV-2 virus ranging from re-purposing the commercially available drugs, using natural compounds, to virtual screening of different databases as well as structure-based approach (Pandey et al., 2021; Quimque et al., 2021; Sharma et al., 2020). These studies targeted different proteins in the life cycle of the virus. Some studies were targeting the human ACE2 protein, others targeted the viral trimeric spike protein, and some targeted the pp1a M^{pro} which is the precursor of all the viral proteins essential in the viral life cycle (Dale et al., 2011; Molchanova et al., 2017; Patrick, 2020; Sachdeva et al., 2019; Sharma et al., 2020). However, no study focused on the use of the peptidomimetics compounds or targeted the Omicron variant using this specific class of compounds.

In this study, we targeted the RBD of the S1 subunit in addition to the stem helix of the S2 subunit of the S protein. This was guided by the interaction of two effective neutralizing monoclonal antibodies. CV3-25 monoclonal antibody inhibits the host-viral membrane fusion by binding to the S2 subunit that is highly conserved among the coronaviruses (Li et al., 2022). EY6A monoclonal antibody binds to the RBD of the S1 subunit preventing its interaction with the human ACE2 enzyme, resulting in preventing the viral access to the human cell (Figure 1) (Zhou et al., 2020). Targeting both S1 and S2 subunits at the same time provides a better chance of halting the viral life cycle. This dual inhibition provides a good strategy to deal with the mutations of the emerging variants. The RBD of the S1 subunit is the main position of the mutations across the different emerging variants. On the other hand, the S2 subunit is not subject to mutations across the different variants providing the possibility of cross-reactivity. Virtual screening of ChEMBL (Davies et al., 2015) and ChemDiv peptidomimetics databases against both the wild type (WT) and the Omicron variant of the SARS-CoV-2 virus was carried out to find compounds with similar biological activity to the antibodies but with better physicochemical activity. The work presented in this study is unique in the use of peptidomimetics to inhibit both the RBD of the S1 subunit and the stem helix of the S2 subunit guided by the interactions of the known monoclonal neutralizing antibodies.

2. Methodology

2.1. Ligand preparation

113,903 compounds and 14,161 compounds were retrieved from ChEMBL and ChemDiv peptidomimetic databases, respectively (Davies et al., 2015). Lipinski's rule of five was applied to the peptidomimetic compounds followed by excluding toxic-moieties containing compounds as well as the removal of pan-assay interference compounds (PAINS) using KNIME (Berthold et al., 2009). This filtration of the peptidomimetics based on the physicochemical properties resulted in 32,667 compounds from the ChEMBL database and 9,062 compounds from the ChemDiv database. These 41,729 peptidomimetic compounds were subjected to a conformational search to account for the flexibility of the ligands and to get the most stable conformations of the molecules using the OMEGA2 package (Hawkins et al., 2010). OMEGA is a knowledge-based method used to produce the bioactive conformations of the molecule.

2.2. Active site preparation and molecular docking

The crystal structures of the RBD of the WT of the SARS-CoV-2 bound with neutralizing antibodies (PDB ID: 7BZ5 (Wu, 2020)) and for the Omicron variant bound with EY6A and Beta-55 monoclonal antibodies (PDB ID: 7QNW (Dejnirattisai et al., 2022)) were obtained from protein data bank (PDB), as well as the crystal structure of the stem helix of the S2 subunit bound with CV3-25 antibody (PDB ID: 7NAB (Li et al., 2022)).

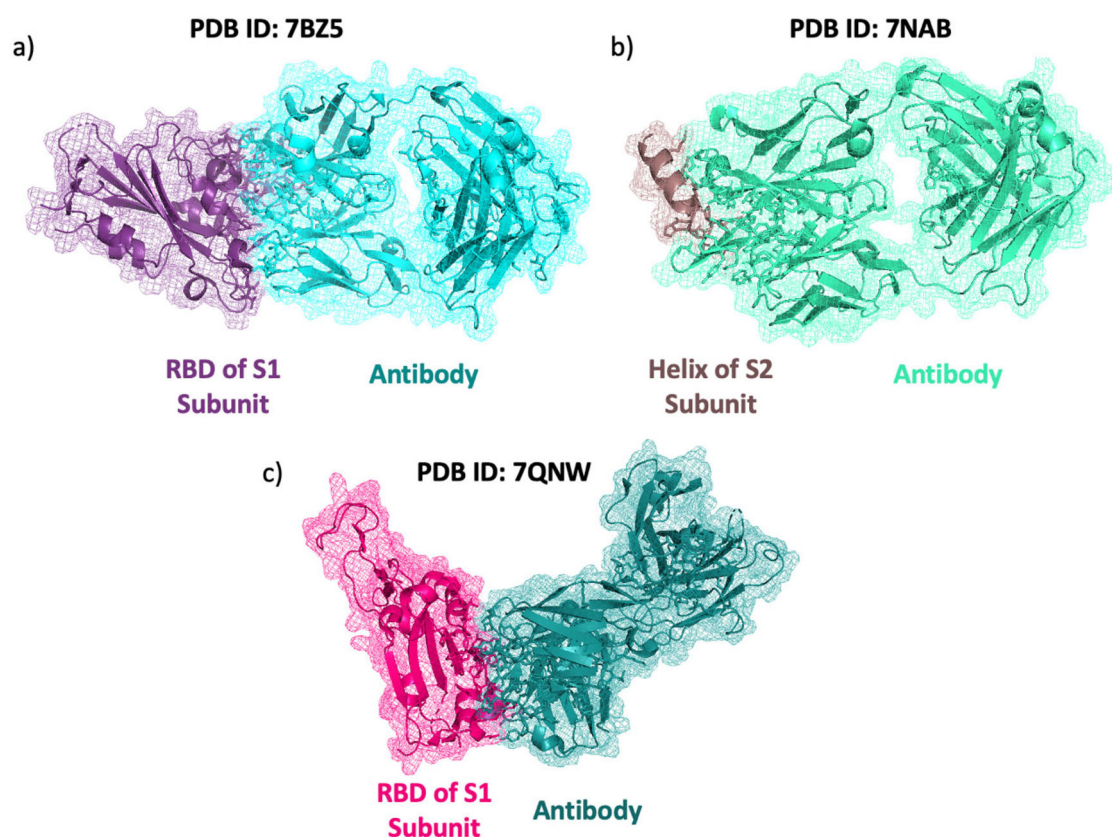


Figure 1. S1 and S2 subunits of the trimeric S glycoprotein augmented with antibodies used for drug targeting in this study. (a) RBD of S1 subunit of WT SARS-CoV-2 virus augmented with antibody (PDB ID: 7BZ5); (b) Stem helix of S2 subunit augmented with antibody (PDB ID: 7NAB); (c) RBD of S1 subunit of Omicron variant of SARS-CoV-2 virus augmented with antibody (PDB ID: 7QNW).

As the goal of this study is to find peptidomimetics with binding modes similar to the neutralizing antibodies of the S glycoprotein, the interacting site of the antibodies with the glycoprotein is considered the docking site. The active sites of the three crystal structures were prepared for docking using the MakeReceptor package (Pandey et al., 2021; Quimque et al., 2021; Sharma et al., 2020). MakeReceptor package depends on generating a negative image for the active site. A negative image is the shape of the active site where ligands bind without clashes (Kelley et al., 2015; McGann, 2011, 2012).

Molecular docking for the 41,729 compounds was employed against the prepared active sites of the two crystal structures of the S1 and S2 subunits of the WT SARS-CoV-2 virus using the FRED package (McGann, 2011, 2012). The top-ranked five molecules targeting the RBD of the S1 subunit were further docked against the RBD of the Omicron variant of SARS-CoV-2 virus. FRED docking method is based on a systematic examination of the possible docking poses, the docked molecules are then arranged concerning the Chemgauss4 scoring function, which depends on shape complementarity (McGann, 2011, 2012).

2.3. Parameterization of the top ranked hits

Restrained Electrostatic potential (RESP) charges of the top-ranked 25 hits based on Chemgauss4 scores of the final peptidomimetics database docked against RBD of WT SARS-CoV-2, Omicron variant, and S2 subunit were calculated using *R.E.D.*

server (Vanqualef et al., 2011). *Ab initio* calculations carried out by *R.E.D.* derives a reproducible partial charge of the non-standard residues independent of the methodology employed in the calculation. The ligands were then parameterized according to the General AMBER force field 2 (GAFF2) using the AnteChamber module (Wang et al., 2001, 2006).

2.4. Molecular dynamics simulations

The ligand-protein complexes of the top-ranked hits were analyzed by molecular dynamics (MD) simulations to evaluate their stability and to calculate the binding free energy. Amber package was used for this purpose, Amber ff14SB force field was used for the protein (Case, 2008; Case et al., 2005; Maier et al., 2015). Each complex was solvated in a cubic water box with a cut-off of 10.0 Å using the TIP3P water model. The system was then neutralized by adding counter charges in the form of Na^+ and Cl^- ions. The steepest descent algorithm was used to minimize the system. This was followed by 50 picoseconds (ps) isothermal-isobaric ensemble (NPT) equilibration at 300 K. A production of 150 nanoseconds (ns) simulations was carried out as canonical ensemble (NVT) in the form of three-independent replicas. A total of $25 \times 150 = 3,750$ ns MD simulations were carried out for the top-ranked 25 protein-ligand complexes.

SHAKE algorithm was applied to all bonds containing hydrogen atoms (Essmann et al., 1995). The Langevin dynamic with the collision frequency 2.0 ps^{-1} was used to couple the systems to a constant temperature of 310 K and a

Table 1. The components of the docking score (shape complementarity, hydrogen bond, protein desolvation, and ligand desolvation) and Chemgauss4 final score of the top ten hits obtained from docking 41,729 compounds from ChEMBL and ChemDiv databases against the S1 subunit of WT SARS-CoV-2 virus using FRED (McGann, 2011, 2012).

| Molecule | Shape complementarity (kcal/mol) | Hydrogen bond (kcal/mol) | Protein desolvation (kcal/mol) | Ligand desolvation (kcal/mol) | Chemgauss4 score (kcal/mol) |
|----------|----------------------------------|--------------------------|--------------------------------|-------------------------------|-----------------------------|
| mol1_S1 | -9.89 | -3.07 | 2.46 | 1.91 | -8.60 |
| mol2_S1 | -9.04 | -3.07 | 2.45 | 1.59 | -8.07 |
| mol3_S1 | -9.24 | -8.48 | 4.00 | 5.80 | -7.92 |
| mol4_S1 | -10.65 | -2.08 | 3.44 | 1.82 | -7.46 |
| mol5_S1 | -10.93 | -1.91 | 3.85 | 1.77 | -7.22 |
| mol6_S1 | -10.75 | -2.19 | 4.04 | 1.82 | -7.08 |
| mol7_S1 | -11.83 | -2.02 | 4.99 | 1.81 | -7.05 |
| mol8_S1 | -9.27 | -3.97 | 3.88 | 2.40 | -6.96 |
| mol9_S1 | -7.46 | -1.44 | 1.44 | 0.57 | -6.89 |
| mol10_S1 | -5.61 | -5.57 | 1.88 | 4.75 | -4.55 |

pressure of 1 bar. The electrostatic interaction was evaluated by the particle-mesh Ewald method (Essmann et al., 1995), and Lennard-Jones interactions were evaluated using 8.0 Å as the cutoff.

2.5. MM/GBSA binding energy calculations

The binding free energy of the top-ranked protein-ligand complexes was calculated using Molecular Mechanics/Generalized Born Surface Area (MM/GBSA) approach (Miller et al., 2012) implemented in AmberTools20 (Case, 2021). The binding free energy of the ligand-protein complex is calculated as the average of the free energy of the three independent replicas (Kollman et al., 2000).

$$\Delta G_{\text{bind}} = \Delta G_{\text{bind, vacuum}} + \Delta G_{\text{solv, complex}} - (\Delta G_{\text{solv, ligand}} + \Delta G_{\text{solv, receptor}}) \quad (1)$$

$$\Delta G_{\text{bind, vacuum}} = \Delta E_{\text{MM}} - T \Delta S \quad (2)$$

MM/GBSA method depends on three components to estimate the binding free energy: the nonbonded interactions between the ligand and the receptor, the solvation free energy electrostatic contribution, and the solvation free energy hydrophobic contribution. The nonbonded interactions between the ligand and the receptor are estimated using molecular mechanics (MM) which depends on the van der Waals and electrostatic interactions ($E_{\text{nonbonded}} = E_{\text{vdw}} + E_{\text{ele}}$). The electrostatic contribution to the solvation free energy is assessed using Generalized Born (GB) method. The hydrophobic contribution to the solvation free energy is calculated using a surface area (SA) term.

2.6. Trajectory analysis

Root-mean-square deviation (RMSD) was calculated to evaluate the stability of the protein-ligand complex and the convergence of the simulations using AmberTools20 (Case, 2021). The first frame of the simulation was considered the reference structure for the RMSD calculations.

$$\text{RMSD} = \sqrt{\frac{1}{N} \sum_{i=1}^N (U r_i - r_i^{\text{ref}})^2} \quad (3)$$

where N is the number of atoms, r_i is the coordinate of atom i , r_i^{ref} is the coordinate of atom i in the reference structure,

and U is the best-fit rotational matrix to align a given structure onto the reference structure.

The binding modes of the top-ranked hits using the initial frame of the 150 ns simulations were explored to compare the interaction of the peptidomimetics to the co-crystallized monoclonal neutralizing antibodies. The stability of the obtained protein-ligand interaction was investigated by calculating the occupancy of the formed hydrogen bonds.

Hydrogen bond analysis for the protein-ligand interaction was carried out over the time course of the 150 ns simulations, a frame was extracted every 100 ps. The analysis was based on the default donor-acceptor distance of 3.0 Å and the default angle of 20° implemented in VMD (Humphrey et al., 1996).

2.7. Principle component analysis

Principle component analysis (PCA) using pair-wise $C\alpha$ distances was carried out to find the main modes of motion of the RBD of the S1 subunit in the MD trajectories of the top-ranked hits. Comparing the explored conformational space of the RBD of the S1 subunit in the WT SARS-CoV-2 virus and the Omicron variant can provide a better understanding of the evasion of the Omicron variant to the immune system.

3. Results and discussion

3.1. Molecular docking

Molecular docking of 41,729 peptidomimetic compounds against the RBD of WT SARS-CoV-2 virus was carried out using FRED (McGann, 2011, 2012) to search for small molecules that have better physicochemical properties than the monoclonal antibodies. Chemgauss4 scores of the top-ranked 10 hits range from -8.60 kcal/mol to -4.55 kcal/mol (Table 1). The shape complementarity component associated with the top 10 hits contributes more to the Chemgauss4 docking score than the hydrogen bond component. This implies that peptidomimetics are similar to antibodies, which rely mainly on the shape complementarity in their binding to the RBD. In addition, the values of protein desolvation are higher than the values of ligand desolvation in most cases. This is attributed to the large protein size when compared to the ligand size.

Table 2. The components of the docking score (shape complementarity, hydrogen bond, protein desolvation, and ligand desolvation) and Chemgauss4 final score of the top ten hits obtained from docking 41,729 molecules from ChEMBL and ChemDiv databases against the S2 subunit of WT SARS-CoV-2 virus using FRED (McGann, 2011, 2012).

| Molecule | Shape complementarity (kcal/mol) | Hydrogen bond (kcal/mol) | Protein desolvation (kcal/mol) | Ligand desolvation (kcal/mol) | Chemgauss 4 score (kcal/mol) |
|----------|----------------------------------|--------------------------|--------------------------------|-------------------------------|------------------------------|
| mol1_S2 | -6.12 | -5.14 | 1.32 | 1.95 | -7.99 |
| mol2_S2 | -4.54 | -5.52 | 0.87 | 1.83 | -7.37 |
| mol3_S2 | -5.08 | -5.00 | 1.16 | 1.57 | -7.36 |
| mol4_S2 | -4.43 | -5.34 | 0.65 | 2.00 | -7.12 |
| mol5_S2 | -5.78 | -4.32 | 1.50 | 1.50 | -7.10 |
| mol6_S2 | -6.80 | -3.46 | 1.35 | 3.11 | -5.80 |
| mol7_S2 | -6.03 | -3.92 | 1.40 | 2.91 | -5.64 |
| mol8_S2 | -5.19 | -4.46 | 1.38 | 2.79 | -5.49 |
| mol9_S2 | -5.26 | -4.49 | 1.42 | 2.89 | -5.45 |
| mol10_S2 | -1.54 | -7.53 | 1.15 | 2.51 | -5.41 |

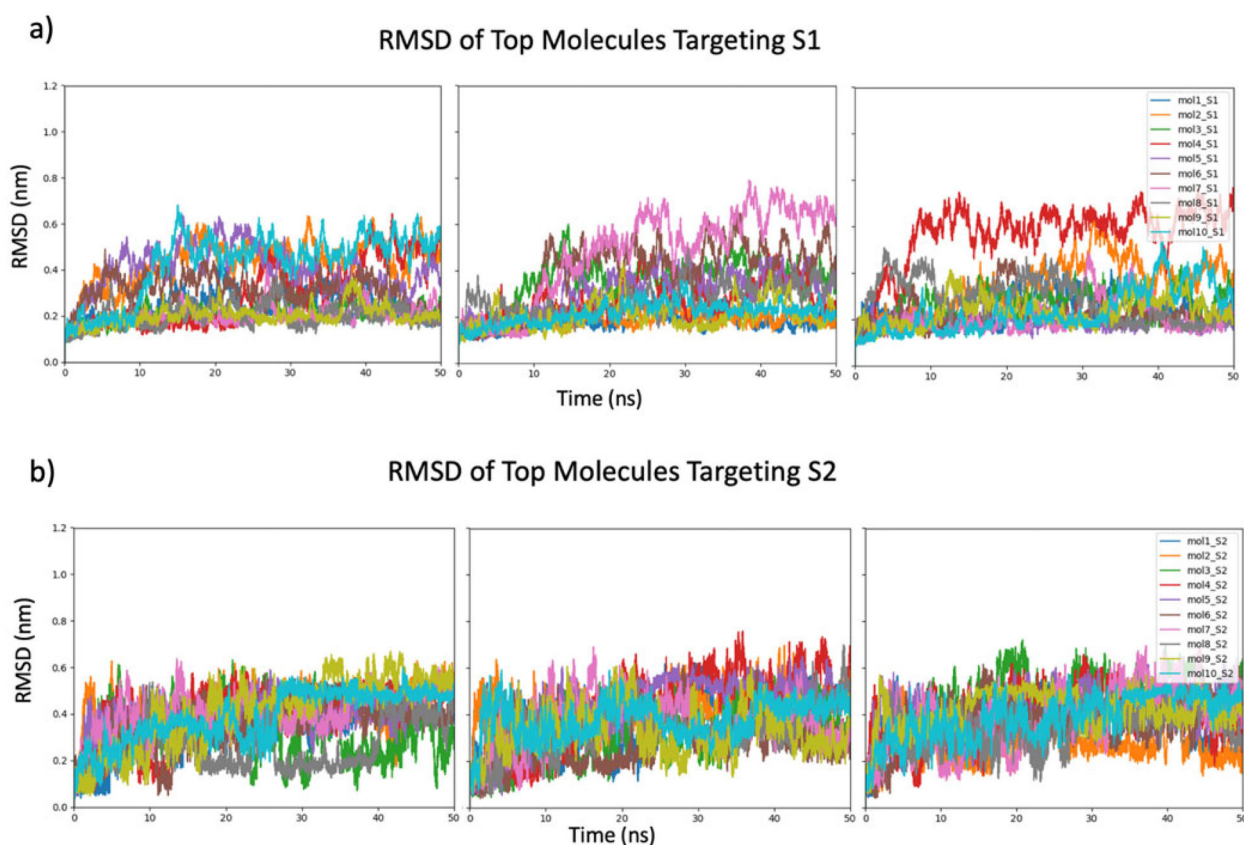


Figure 2. RMSD of the molecular dynamics simulations of the top ten protein-ligand complexes from the docking processes. (a) RMSD of the top-ranked ten hits targeting the RBD of S1 subunit of WT of SARS-CoV-2 virus; (b) RMSD of the top-ranked ten hits targeting the stem helix of S2 subunit of S trimeric glycoprotein.

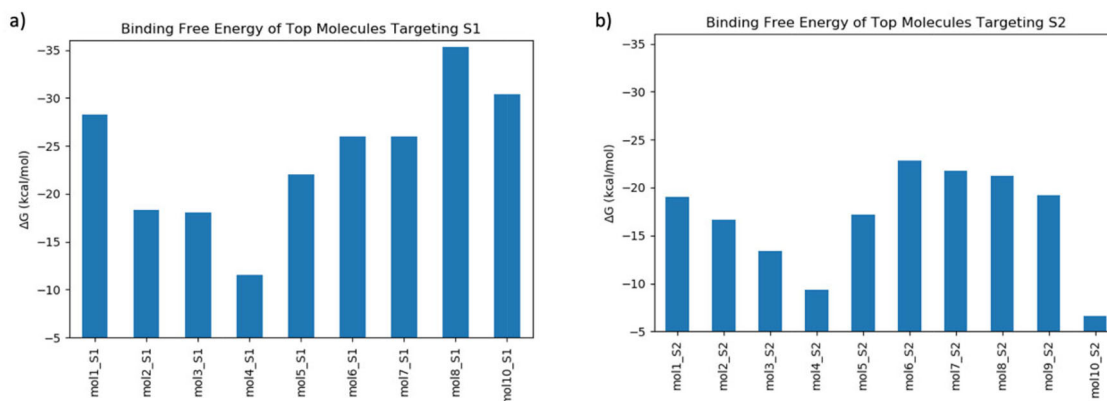


Figure 3. The binding free energies of the top ligands targeting both S1 and S2 subunits of S glycoprotein. (a) The binding free energy of the top nine hits targeting the RBD of the S1 subunit, ranging between -11 kcal/mol and -36 kcal/mol. Ligand mol9_S1 was not plotted as it was associated with positive binding free energy. (b) The binding free energies of the top ten hits targeting the stem helix of the S2 subunit, ranging between -6 kcal/mol and -25 kcal/mol.

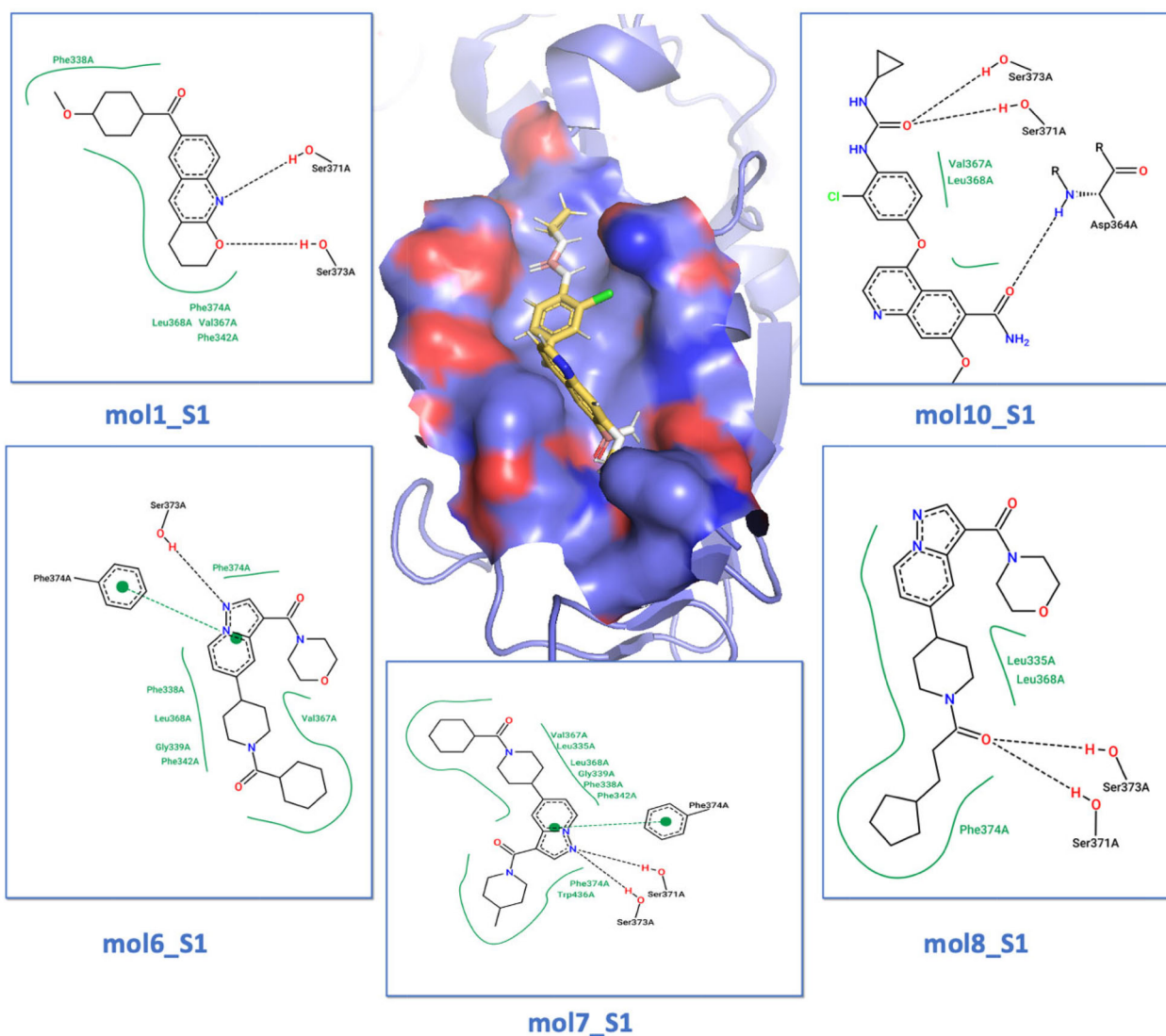


Figure 4. The binding mode of the top 5 hits, with binding energy higher, more negative, than -25 kcal/mol, targeting the RBD of the S1 subunit of WT SARS-CoV-2. The 2D interactions are generated by the PoseView interface (Stierand et al., 2006).

The molecular docking of the final peptidomimetics database against the stem helix of the S2 subunit of the SARS-CoV-2 Virus is guided by the interaction of the CV3-25 antibody. The Chemgauss4 scores of the top10 hits range from -7.99 kcal/mol to -5.41 kcal/mol (Table 2). Both shape complementarity and hydrogen bond component contribute to the final docking score of the ranked top 10 hits. This implies the importance of both components for the ligands to interact effectively with the stem helix of the S2 subunit. The contribution of the ligand desolvation and protein desolvation components to the final docking score varies from one ligand to the other (Table 2). This may be attributed to the small size of the target.

3.2. Molecular dynamics simulations

150 ns MD simulations were carried out as three independent 50 ns trajectories for each of the top10 hits resulting from the molecular docking process. MD simulations were carried out to allow both protein and ligand to be free and explore different conformational spaces in their bound state. RMSD

was calculated with respect to the first frame of the simulations. The fluctuation of the RMSD values in the three independent 50 ns trajectories for each of the top-ranked ten hits obtained from docking of the peptidomimetics database against the RBD of the S1 subunit of WT SARS-CoV-2 virus ranged between 0.2 and to 0.6 nm for all the ligands, where the deviation of the RMSD values for each ligand is less than 0.1 nm (Figure 2a). This small fluctuation indicates the convergence of the simulations and the stability of the binding mode between the ligand and the protein. Similarly, the MD simulations of the top-ranked ten hits obtained from molecular docking of the peptidomimetics against the stem helix of the S2 subunit were associated with small RMSD fluctuations, also ranging between 0.2 and 0.6 nm. These also indicate the stability of the ligand binding and the convergence of the simulations (Figure 2b).

3.3. MM/GBSA binding energy calculations

The binding free energies of the top hits targeting the RBD of the S1 subunit and the stem helix of the S2 subunit, 10

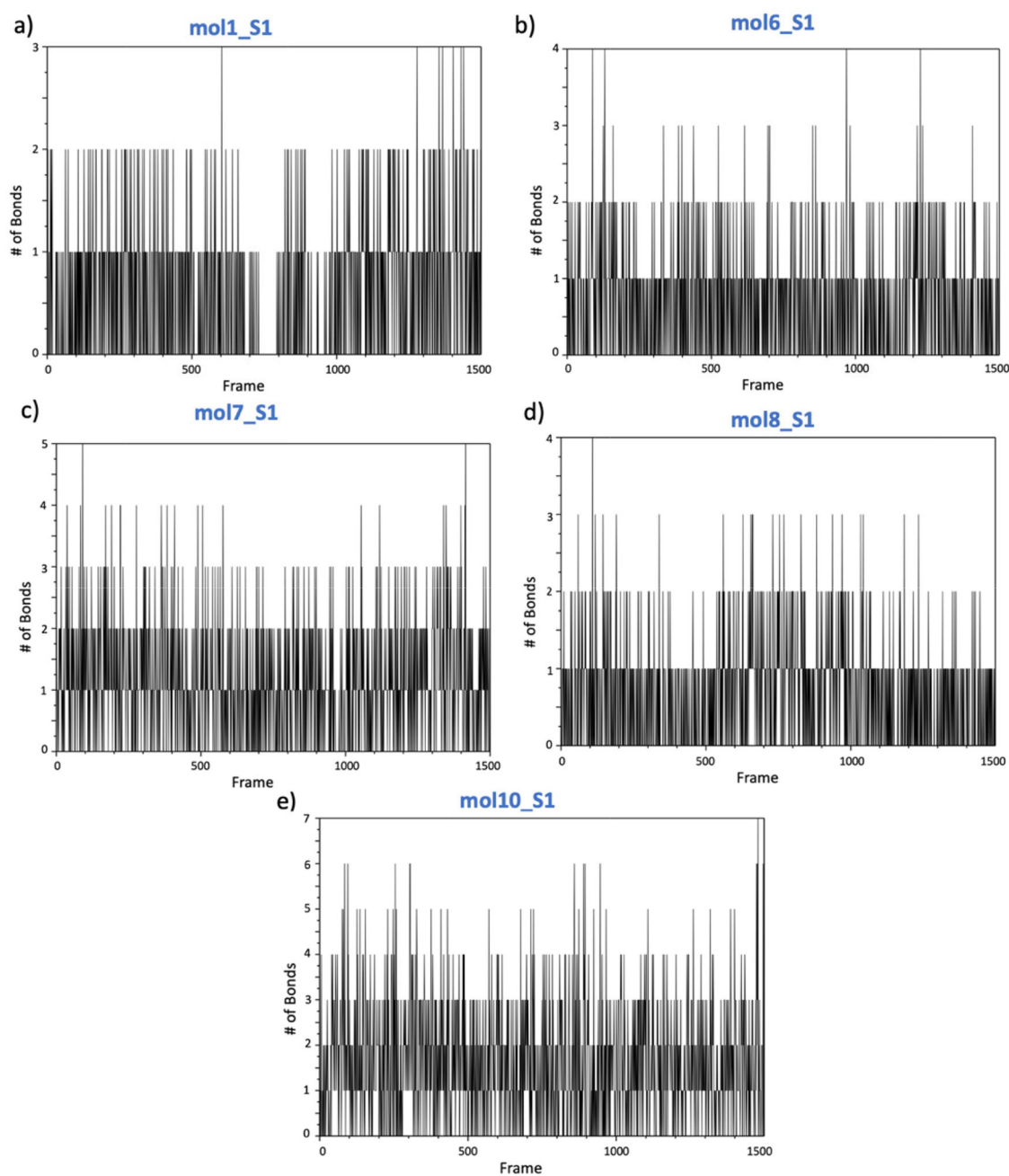


Figure 5. Hydrogen bond analysis of the top 5 hits, with binding energy higher than -25 kcal/mol, targeting the RBD of the S1 subunit of WT SARS-CoV-2.

each, were calculated using MM/GBSA method. The reported binding free energy is the average of the binding energy calculated from the three independent 50 ns simulations for each ligand. The binding free energies of ligands targeting RBD of the S1 subunit range from -11 to -36 kcal/mol (Figure 3a). The ligands with binding free energy higher, more negative, than -25 kcal/mol were selected to further evaluate their binding mode. The binding free energies of the molecules targeting the stem helix of the S2 subunit were lower than those targeting the RBD (indicating weaker interactions), where the binding free energies range from -6 kcal/mol to -25 kcal/mol (Figure 3b). The ligands with binding free energies higher, more negative, than -19 kcal/mol were selected to further evaluate their binding mode with the stem helix.

3.4. Binding mode analysis

The fluctuations in the RMSD values of the top five compounds targeting the RBD of the S1 subunit, with binding free energy higher than -25 kcal/mol, were found to be less than 1 \AA . This indicates the stability of the interaction between the protein and the ligand. The top five compounds were structurally similar to each other and thus were expected to have similar binding modes. The first frame of the 150 ns MD simulation was utilized to investigate the binding mode of the top-ranked five hits. All five compounds form a hydrogen bond with residues Ser373 and Ser371, except for mol6_S1, which forms a hydrogen bond with Ser373 only (Figure 4). Additional π - π stacking is formed with Phe374 by both mol6_S1 and mol7_S1. Compound

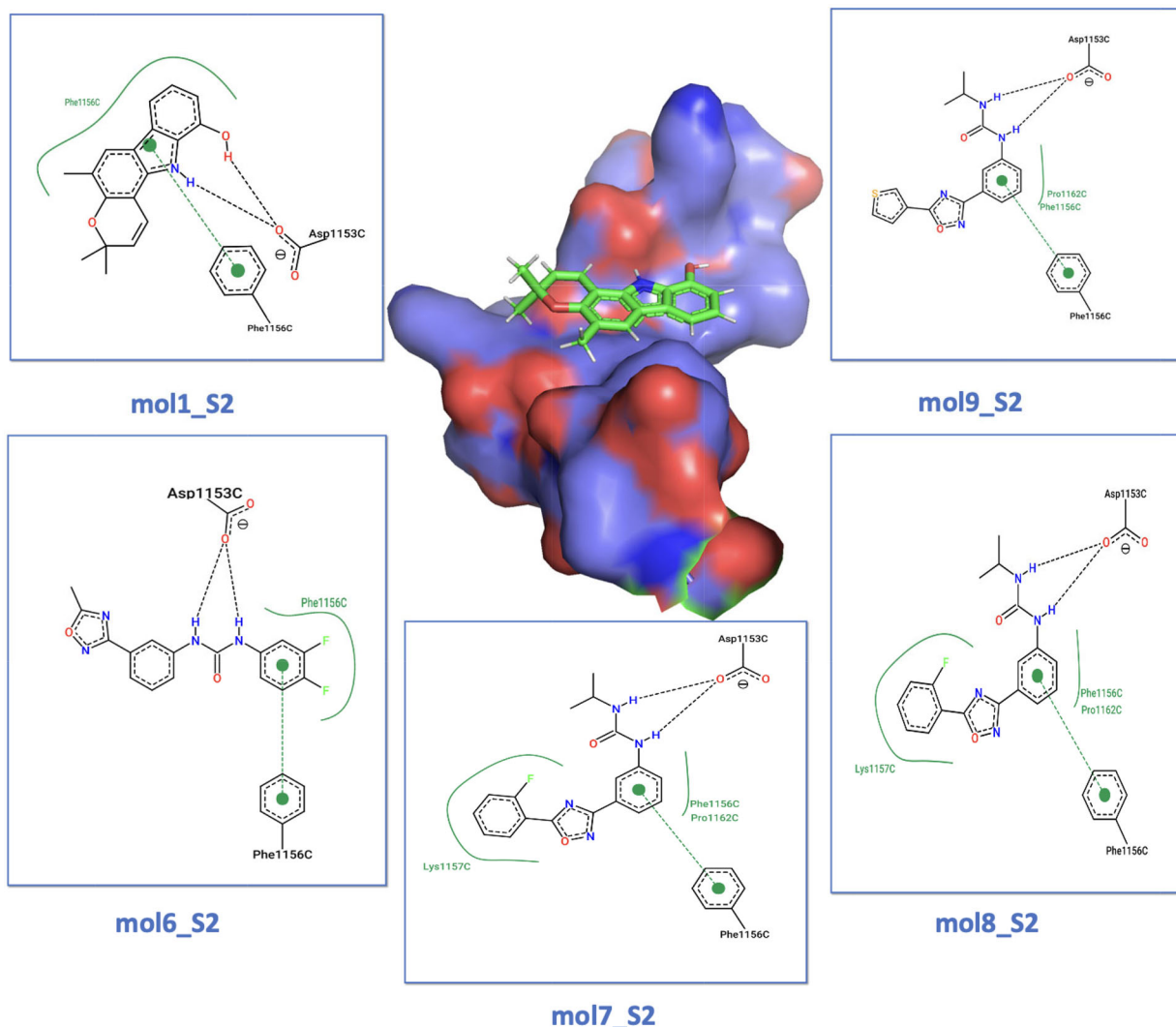


Figure 6. The binding mode of the top 5 hits, with binding energy higher than -19 kcal/mol, targeting the stem helix of the S2 subunit of WT SARS-CoV-2. The 2D interactions are generated by the PoseView interface (Stierand et al., 2006).

mol10_S1 forms a unique hydrogen bond with Asp364, which is not found in the other four compounds (Figure 4). Both Val367 and Leu368 were in close contact with these top-ranked five compounds.

The top five hits share the same active site as EY6A monoclonal antibody. However, the binding modes of these top five ligands against RBD of the S1 subunit are quite different. The light and the heavy chains of the EY6A monoclonal antibody form bonds with different residues including Tyr369, Phe377, Leu378, Gly381, Val382, Ser383, and Pro384 (Zhou et al., 2020). These residues are in proximity to the residues the top 5 hits peptidomimetics interact. In other words, they share the same active site but form different interactions. The common interaction of the top-ranked peptidomimetics with Ser373 in the RBD highlights the importance of other non-interacting residues with EY6A monoclonal antibody in the same active site. To further elucidate the importance of this residue, the distance distribution of the top-ranked hits targeting the RBD and Ser373 was explored (Figure S3). The small variation in the distance along the simulations indicates the stability of the binding between the top hits and Ser373.

The stability of the formed hydrogen bonds between the top five hits and the RBD of the S1 subunit was investigated by calculating the frequency of the hydrogen bond over the time course of the entire trajectory. The top-ranked five hits were found to form three hydrogen bonds in mol1, four hydrogen bonds in mol6 and mol8, five hydrogen bonds in mol7, and seven hydrogen bonds in mol10. Two hydrogen bonds in complexes formed with mol1, mol6, and mol8, and three hydrogen bonds in complexes formed with mol7 and mol10 were found to be stable over the time course of 150 ns simulation (Figure 5). The occupancy of two hydrogen bonds, represented as the percent of frames that form at least two hydrogen bonds, in mol 1, mol6, and mol8 were 63.4%, 62.2%, and 58.8%, respectively. The occupancy of three hydrogen bonds in mol7 was 37%, and in mol10 was 46.2%. The high occupancy of double hydrogen bonds in mol1, mol6, and mol8 and of triple hydrogen bonds in mol7 and mol10 support that the binding mode of the top five hits indicated in Figure 4 as the most probable binding mode.

The RMSD values of the top five compounds, with binding free energy higher than -19 kcal/mol, targeting the stem helix of the S2 subunit are less than 1 Å. This reflects the stability of

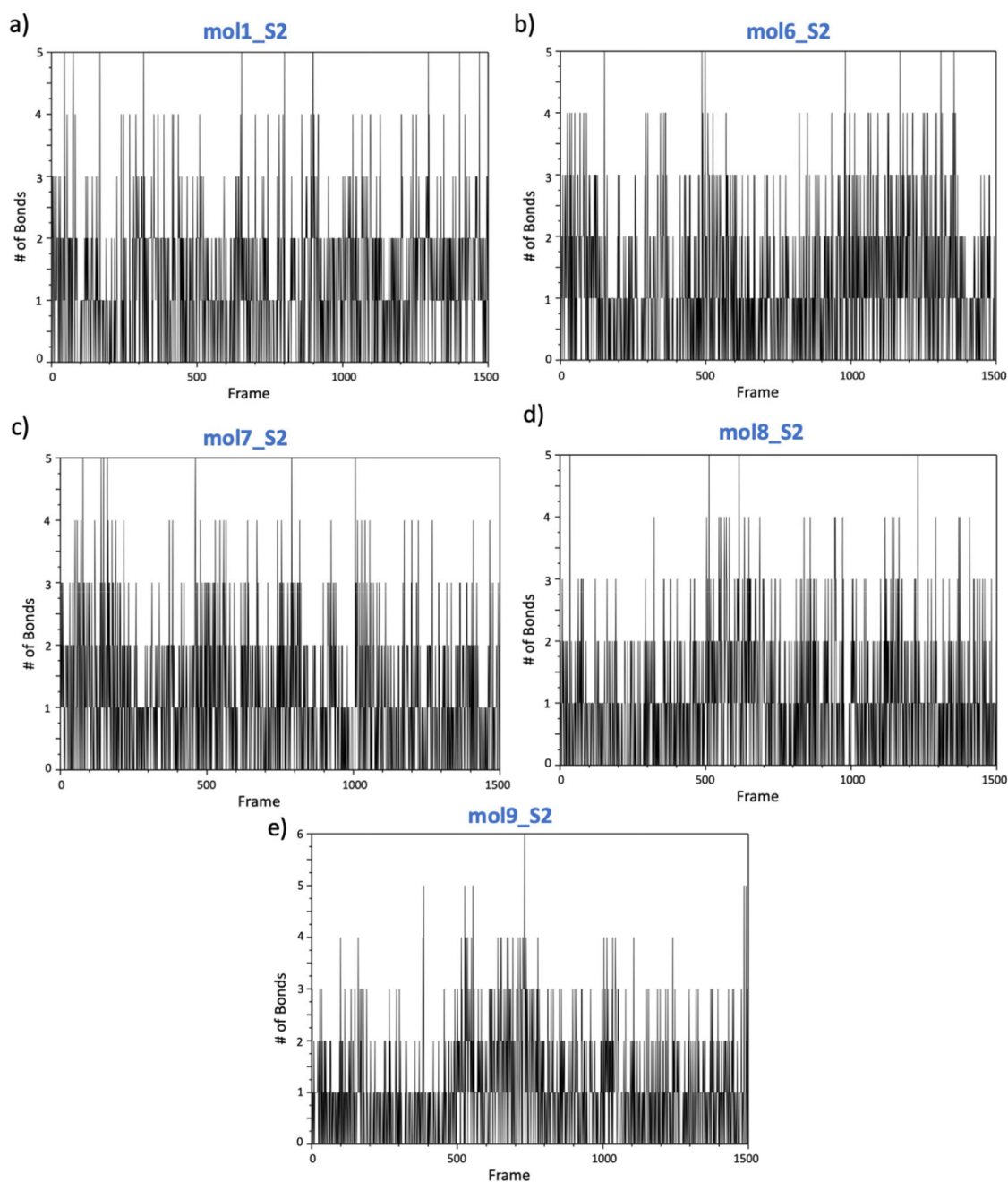


Figure 7. Hydrogen bond analysis of the top 5 hits, with binding energy higher than -19 kcal/mol, targeting the stem helix of the S2 subunit of WT SARS-CoV-2.

Table 3. The components of the docking score (shape complementarity, hydrogen bond, protein desolvation, and ligand desolvation) and Chemgauss4 final score of the top five hits against the S1 subunit of Omicron SARS-CoV2 virus using FRED (McGann, 2011, 2012).

| Molecule | Shape complementarity (kcal/mol) | Hydrogen bond (kcal/mol) | Protein desolvation (kcal/mol) | Ligand desolvation (kcal/mol) | Chemgauss 4 score (kcal/mol) |
|----------|----------------------------------|--------------------------|--------------------------------|-------------------------------|------------------------------|
| mol1_S1 | -7.90 | -0.19 | 2.49 | 0.88 | -4.72 |
| mol6_S1 | -7.21 | -0.20 | 3.60 | 0.91 | -2.91 |
| mol8_S1 | -7.25 | -0.06 | 3.89 | 0.97 | -2.45 |
| mol10_S1 | -5.15 | -5.04 | 2.88 | 4.59 | -2.72 |

the interaction between the top hits and the target protein. The binding modes of the top five compounds, based on the initial frame of the simulations, targeting the stem helix of the S2 subunit were very similar to each other (Figure 6). All five compounds form a hydrogen bond with Asp1153 and π - π stacking bond with Phe1156. Phe1156 and Pro1162 are in close contact with the top hits targeting the stem helix. This

suggests the importance of these residues in the development of effective inhibitors against the stem helix of the S2 subunit. These compounds could provide cross-reactivity across the different variants of the SARS-CoV-2 virus as they inhibit the conserved S2 subunit, which is not subject to mutations.

The binding modes of the top five peptidomimetics hits are similar to CV3-25 Fabs that interact with the hydrophobic face

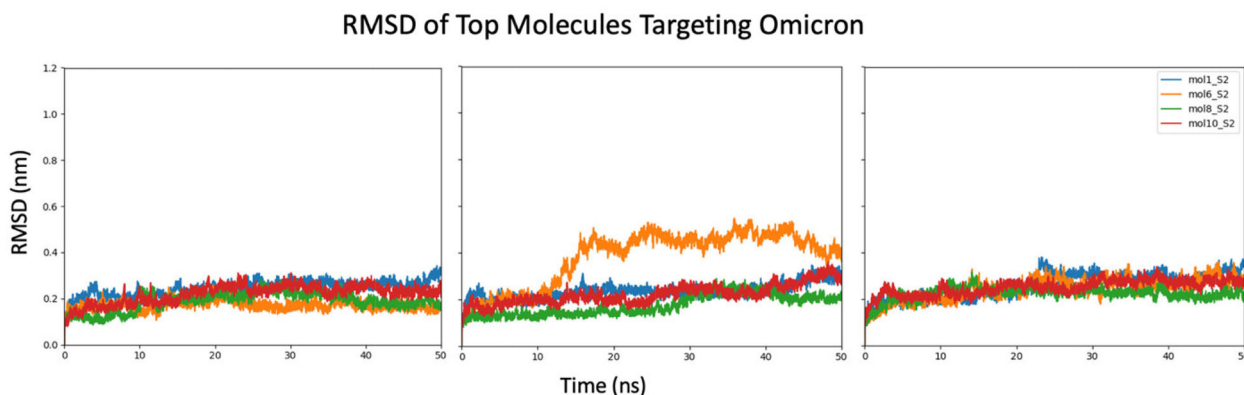


Figure 8. RMSD of the three independent 50 ns molecular dynamics simulations of the top-ranked 4 hits targeting the RBD of the Omicron variant of SARS-CoV-2 virus.

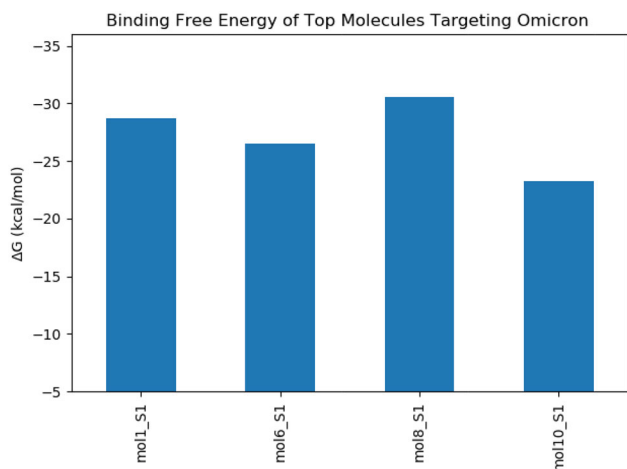


Figure 9. The binding free energy of the top-ranked four hits targeting the RBD of the Omicron variant of the SARS-CoV-2 virus.

of the stem helix by forming a bond with the charged residues Asp1153 and Lys1157 (Li et al., 2022). All five compounds form hydrogen bonds with charged Asp1153. Lys1157 residue is in close contact with mol7_S2 and mol8_S2. This implies the likelihood of these molecules as good inhibitors against the stem helix of the S2 subunit as they share the same binding mode of CV3-25 Fabs. The same binding mode highlights the importance of the role of Asp1153 residue in the S2 subunit across the different variants of the SARS-CoV-2 virus for the possibility of cross-reactivity. The distance distribution of the top-ranked hits and the Asp1153 in the stem helix of the S2 subunit was calculated to investigate the stability of the identified binding mode (Figure S4). The small deviation in the distance along the simulation reflects the stability of the identified binding mode of the top-ranked hits. This highlights the importance of Asp1153 in the interaction of effective inhibitors against the S2 subunit.

The binding modes of the top-ranked five hits targeting the stem helix of the S2 subunit were further validated by the frequency of the hydrogen bond over the time course of the simulations. All the top-ranked five hits form 5 hydrogen bonds, except for mol9 which forms six hydrogen bonds (Figure 7). Only three hydrogen bonds were found to be the most stable in all the top-ranked five hits. The binding mode of the triple hydrogen bonds in the top-ranked five hits

targeting the stem helix of the S2 subunit occupies at least 40% of the simulation time. The persistence percent, occupancy, of the formed three hydrogen bonds in mol1 was 37%, in mol6 was 76.3%, in mol7 was 49.1%, in mol8 was 52.8%, and in mol9 was 51.4%. This reflects that the binding mode including three hydrogen bonds is the most abundant. This agrees with the suggested binding modes in Figure 6.

3.5. Targeting the RBD of the Omicron variant of SARS-CoV-2 virus

3.5.1. Molecular docking

The top five molecules targeting the RBD of the S1 subunit of WT SARS-CoV-2 virus were docked against the RBD of the Omicron variant of SARS-CoV-2 virus (PDB ID: 7QNW) to check their effectiveness against the new variant of SARS-CoV-2 virus. The active site used in the molecular docking was the interaction site between the RBD and the EY6A monoclonal antibody (similar to the one used in the case of the WT SARS-CoV-2). Molecular docking employed by the FRED package (McGann, 2011, 2012) showed a lower Chemgauss4 docking score when compared to the scores obtained from the molecular docking against the RBD of the WT SARS-CoV-2 virus (Table 3). These lower docking scores were observed in four of the five top-ranked hits, except for mol7_S1, which exerts no interaction with the active site. Shape complementarity was found to be the largest component of the final docking score. The contribution of the protein desolvation was much higher than the ligand desolvation to the final docking score (Table 3), similar to the docking results against the WT virus (Table 1).

3.5.2. Molecular dynamics simulations

RMSD was calculated over the time course of 150 ns molecular dynamics simulations, carried out in the form of three independent trajectories, for the top-ranked four hits targeting the RBD of the Omicron variant of SARS-CoV-2 virus. The RMSD fluctuations of these simulations range between 0.2 nm and 0.3 nm, except for replica 2 for which the RMSD fluctuations range from 0.2 nm to 0.4 nm (Figure 8). These small RMSD fluctuations indicate the stability of the protein-ligand binding.

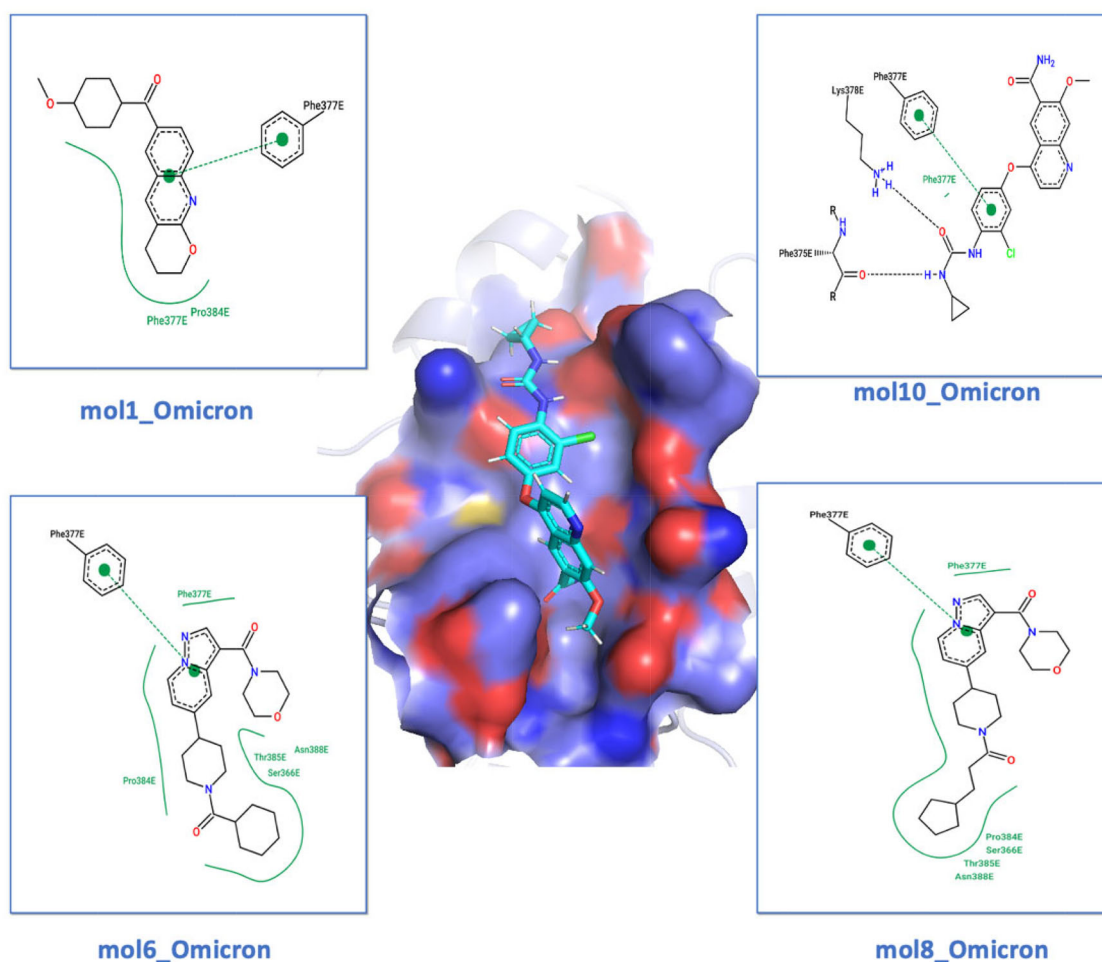


Figure 10. The binding mode analysis of the top-ranked four hits targeting the RBD of the Omicron variant of the SARS-CoV-2 virus. The 2D interactions are generated by PoseView interface (Stierand et al., 2006).

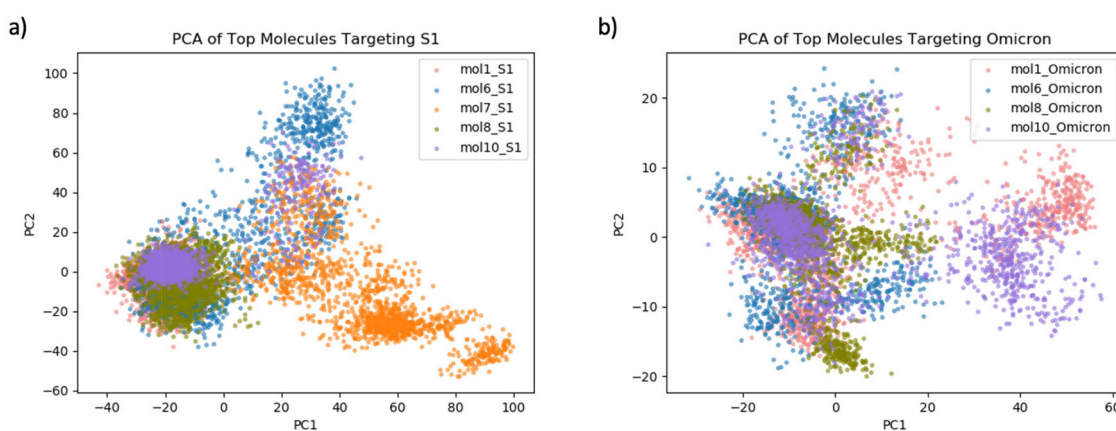


Figure 11. PCA of the RBD of the S1 subunit in the MD trajectories of the top-ranked hits. (a) Explored conformational space of the RBD of the WT SARS-CoV-2 virus. (b) Explored conformational space of the RBD of the Omicron variant.

3.5.3. MM/GBSA calculations

The binding free energies of the top-ranked four compounds were estimated as the average of the binding free energy calculated from the three independent 50 ns trajectories using the MM/GBSA method. There was a slight decrease in the binding free energy of the top-ranked four hits targeting the RBD of the Omicron variant of the SARS-CoV-2 virus (Figure 9) when compared to the binding free energy of the same molecules targeting the RBD of the WT of SARS-CoV-2

virus (Figure 3a). This is consistent with the results of the molecular docking (Table 3) where lower Chemgauss4 docking scores were observed.

3.5.4. Binding mode analysis

The binding modes of the four top-ranked targeting the RBD of the Omicron variant, obtained from the first frame of the simulations, were analyzed to insinuate the cause of the

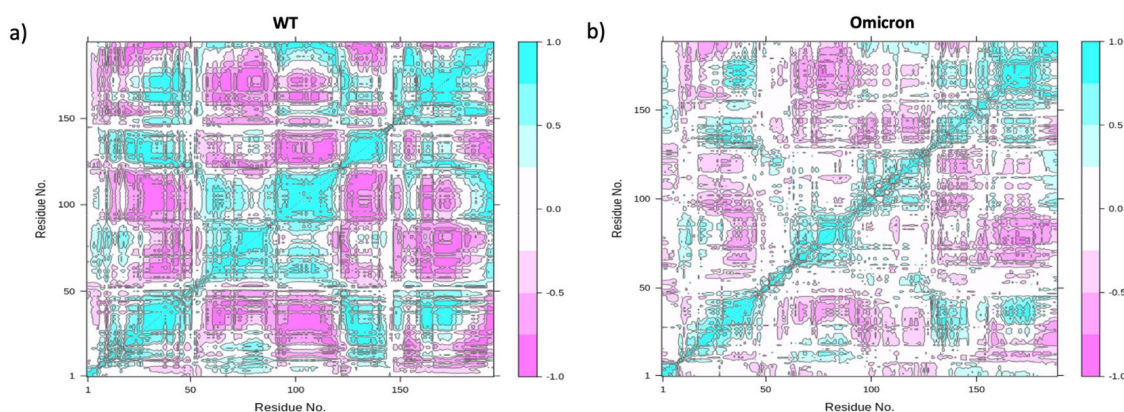


Figure 12. Dynamical Cross-Correlation Matrix (DCCM) of the RBD of the S1 subunit generated by Bio3d (Grant et al., 2006). (a) Cross-correlation of the residues of the RBD of the WT SARS-CoV-2 virus; (b) cross-correlation of the residues of the RBD of the Omicron variant of SARS-CoV-2 virus.

decrease of the binding free energy when compared to the WT. The binding mode analysis showed that all the top four compounds form π - π stacking interaction with Phe377 (Figure 10). In addition, Pro384 was in close contact with the ligands. These compounds lack the interaction with Ser371 and Ser373, which form prominent interactions with these compounds in the cases of the RBD of the WT of the SARS-CoV-2 virus. On the other hand, these binding modes of the top 4 hits are similar to the binding mode EY6A monoclonal antibody (Zhou et al., 2020). Despite the slight decrease in the binding free energies and the different binding modes against the Omicron variant of the SARS-CoV-2 virus, these top-ranked four hits are expected to be effective in inhibiting the RBD of the trimeric S glycoprotein with a minimum binding free energy of -20 kcal/mol (Figure 9).

3.6. Insight into the effect of the mutation in WT and the Omicron variant of the SARS-CoV-2 virus

The mutations in the RBD of the S protein altered the binding mode of the top-ranked hits as indicated by the 2D interactions and the frequency of the hydrogen bonds over the time course of the 150 ns simulations. PCA was implied as a dimension reduction technique using pair-wise $C\alpha$ distances to compare the conformational spaces explored by the RBD in both the WT and Omicron variant. The explored conformational space of the protein associated with the top-ranked hits in the case of the WT was found to be distinctive from each other (Figure 11a). On the other hand, the explored conformational space of the protein in the case of the Omicron variant overlapped with each other (Figure 11b).

Dynamical Cross-Correlation Matrix (DCCM) was employed to analyze the correlated conformational of the RBD in the WT and the Omicron variant of the SARS-CoV-2 virus. High positive correlations indicate strongly correlated motions between the residues of the N-terminal and residues 1–50 of the RBD of the WT (Figure 12a). This strongly correlated motion is reduced immensely in the case of the Omicron variant (Figure 12b). Residues 50–100 were associated with a high negative cross-correlation with residues 1–50 (Figure 12a). This negative cross-correlation indicates that the movement of these two regions of the protein is opposite to each

other. The motion of these regions in the Omicron variant was found to be much less correlated (Figure 12b). DCCM shows that the mutations in the RBD highly affected the correlated motion between the different regions of the RBD of the S1 subunit.

4. Conclusion

In conclusion, the global pandemic caused by SARS-CoV-2 virus is still an issue of concern due to the emerging Omicron variant that evades the immune system. It is important to find potent inhibitors that are effective against both the WT and the Omicron variant. The developed vaccines are based on immunogens of S trimeric glycoprotein. S glycoprotein is essential in the life cycle of the SARS-CoV-2 virus to facilitate the binding and the membrane fusion to the host receptors using the S1 and S2 subunits, respectively.

In this study, molecular docking of nearly 42,000 peptidomimetic compounds was carried out against the RBD of the S1 subunit of both WT and Omicron variants of SARS-CoV-2 virus and the stem helix of the S2 subunit guided by the interaction of effective monoclonal neutralizing antibodies: EY6A and CV3-25, respectively. The top-ranked hits with respect to the Chemgauss 4 docking score were subject to molecular dynamics simulations to explore more conformational space. Five hits were found to be effective against the RBD of WT SARS-CoV-2 virus with binding free energy higher than -25 kcal/mol. Four of these five hits were found to be effective against the RBD of the Omicron variant with binding free energy higher than -20 kcal/mol. Moreover, five ligands were identified to inhibit the stem helix of the S2 subunit with binding free energy higher than -19 kcal/mol.

The binding mode analysis of the top ligands insinuates the role of different residues as Ser371 and Ser373 in the RBD of WT SARS-CoV-2 virus and Phe377 in the RBD of the Omicron variant in the effective interaction of the ligands. Asp1153 and Phe1156 were elucidated to be essential for the interaction of the peptidomimetic inhibitors with the stem helix of the S2 subunit. Further studies should be carried out to investigate the role of these residues in the life cycle of the SARS-CoV-2 virus and its emerging Omicron variant.

Acknowledgments

The authors would like to thank Tingting Zhao and Mohamed Ali Elrefaiy for their help with the manuscript. Computational time was provided by Southern Methodist University's Center for Research Computing.

Experimental data

The crystal structure of SARS-CoV-2 spike protein (PDB IDs: 7BZ5, 7NAB, and 7QNW) can be obtained free of charge from the Protein Data Bank (<https://www.rcsb.org/>).

Packages

KNIME package can be downloaded free of charge from (<https://www.knime.com/>).

MakeReceptor module, Omega, and FRED can be obtained from OpenEye Scientific using (<https://www.eyesopen.com>).

Disclosure statement

The authors declare no competing financial interest.

Funding

Research reported in this paper was supported by the National Institute of General Medical Sciences of the National Institutes of Health under Award no. R15GM122013.

ORCID

Peng Tao  <http://orcid.org/0000-0002-2488-0239>

References

- Baden, L. R. (2020). Efficacy and safety of the mRNA-1273 SARS-CoV-2 vaccine. *New England Journal of Medicine*, 384(5), 403–416.
- Berthold, M. R., Cebren, N., Dill, F., Gabriel, T. R., Kötter, T., Meinel, T., Ohl, P., Thiel, K., & Wiswedel, B. (2009). KNIME-the Konstanz information miner: Version 2.0 and beyond. *ACM SIGKDD Explorations Newsletter*, 11(1), 26–31. <https://doi.org/10.1145/1656274.1656280>
- Campbell, F., Archer, B., Laurenson-Schafer, H., Jinnai, Y., Konings, F., Batra, N., Pavlin, B., Vandemaale, K., Van Kerkhove, M. D., Jombart, T., Morgan, O., & le Polain de Waroux, O. (2021). Increased transmissibility and global spread of SARS-CoV-2 variants of concern as at June 2021. *Eurosurveillance*, 26(24), 2100509. <https://doi.org/10.2807/1560-7917.ES.2021.26.24.2100509>
- Case, D. A. (2008). *Amber 10*. San Francisco: University of California.
- Case, D. A. (2021). *Amber*. University of California.
- Case, D. A., Cheatham, T. E., Darden, T., Gohlke, H., Luo, R., Merz, K. M., Onufriev, A., Simmerling, C., Wang, B., & Woods, R. J. (2005). The Amber biomolecular simulation programs. *Journal of Computational Chemistry*, 26(16), 1668–1688. <https://doi.org/10.1002/jcc.20290>
- Colmenares-Mejía, C. C., Serrano-Díaz, N., Quintero-Lesmes, D. C., Meneses, L., Salazar Acosta, I., Idrovo, Á. J., Sanabria-Echeverry, D. Y., Cordero-Rebolledo, H., & Castillo, V. (2021). Seroprevalence of SARS-CoV-2 infection among occupational groups from the Bucaramanga metropolitan area, Colombia. *International Journal of Environmental Research and Public Health*, 18(8), 4172. <https://doi.org/10.3390/ijerph18084172>
- Cowell, S. M., Lee, Y. S., Cain, J. P., & Hruby, V. J. (2004). Exploring Ramachandran and chi space: Conformationally constrained amino acids and peptides in the design of bioactive polypeptide ligands. *Current Medicinal Chemistry*, 11(21), 2785–2798. <https://doi.org/10.2174/0929867043364270>
- Cui, J., Li, F., & Shi, Z.-L. (2019). Origin and evolution of pathogenic coronaviruses. *Nature Reviews. Microbiology*, 17(3), 181–192. <https://doi.org/10.1038/s41579-018-0118-9>
- Dale, J. W., Hollingworth, G. J., & McKenna, J. M. (2011). Developments and advances in gastrointestinal prokinetic agents. In *Annual reports in medicinal chemistry* (Vol. 46, pp. 135–154). Elsevier.
- Davies, M., Nowotka, M., Papadatos, G., Dedman, N., Gaulton, A., Atkinson, F., Bellis, L., & Overington, J. P. (2015). ChEMBL web services: Streamlining access to drug discovery data and utilities. *Nucleic Acids Research*, 43(W1), W612–W620. <https://doi.org/10.1093/nar/gkv352>
- Dejnirattisai, W., Huo, J., Zhou, D., Zahradník, J., Supasa, P., Liu, C., Duyvesteyn, H. M., Ginn, H. M., Mentzer, A. J., Tuekprakhon, A., Nutalai, R., Wang, B., Djokaite, A., Khan, S., Avinoam, O., Bahar, M., Skelly, D., Adele, S., Johnson, S. A., ... Young, P. (2022). SARS-CoV-2 Omicron-B. 1.1. 529 leads to widespread escape from neutralizing antibody responses. *Cell*, 185(3), 467–484.e15. <https://doi.org/10.1016/j.cell.2021.12.046>
- Du, X. (2022). Omicron adopts a different strategy from Delta and other variants to adapt to host. *Transduction and Targeted Therapy*, 7(1), 1–3.
- Essmann, U., Perera, L., Berkowitz, M. L., Darden, T., Lee, H., & Pedersen, L. G. (1995). A smooth particle mesh Ewald method. *Journal of Chemical Physics*, 103(19), 8577–8593. <https://doi.org/10.1063/1.470117>
- Grant, B. J., Rodrigues, A. P. C., ElSawy, K. M., McCammon, J. A., & Caves, L. S. D. (2006). Bio3d: An R package for the comparative analysis of protein structures. *Bioinformatics (Oxford, England)*, 22(21), 2695–2696. <https://doi.org/10.1093/bioinformatics/btl461>
- Hawkins, P. C. D., Skillman, A. G., Warren, G. L., Ellingson, B. A., & Stahl, M. T. (2010). Conformer generation with OMEGA: Algorithm and validation using high quality structures from the Protein Databank and Cambridge Structural Database. *Journal of Chemical Information and Modeling*, 50(4), 572–584. <https://doi.org/10.1021/ci100031x>
- He, M., Wang, Y., Huang, S., Zhao, N., Cheng, M., & Zhang, X. (2021). Computational exploration of natural peptides targeting ACE2. *Journal of Biomolecular Structure and Dynamics*. <https://doi.org/10.1080/07391102.2021.1905555>
- Hoffmann, M., Arora, P., Groß, R., Seidel, A., Hörnich, B. F., Hahn, A. S., Krüger, N., Graichen, L., Hofmann-Winkler, H., Kempf, A., Winkler, M. S., Schulz, S., Jäck, H.-M., Jahrsdörfer, B., Schrezenmeier, H., Müller, M., Kleger, A., Münch, J., & Pöhlmann, S. (2021). SARS-CoV-2 variants B. 1.351 and P. 1 escape from neutralizing antibodies. *Cell*, 184(9), 2384–2393. <https://doi.org/10.1016/j.cell.2021.03.036>
- Hoffmann, M., Kleine-Weber, H., Schroeder, S., Krüger, N., Herrler, T., Erichsen, S., Schiergens, T. S., Herrler, G., Wu, N.-H., Nitsche, A., Müller, M. A., Drosten, C., & Pöhlmann, S. (2020). SARS-CoV-2 cell entry depends on ACE2 and TMPRSS2 and is blocked by a clinically proven protease inhibitor. *Cell*, 181(2), 271–280. <https://doi.org/10.1016/j.cell.2020.02.052>
- Humphrey, W., Dalke, A., & Schulten, K. (1996). VMD: Visual molecular dynamics. *Journal of Molecular Graphics*, 14(1), 33–38. [https://doi.org/10.1016/0263-7855\(96\)00018-5](https://doi.org/10.1016/0263-7855(96)00018-5)
- Kelley, B. P., Brown, S. P., Warren, G. L., & Muchmore, S. W. (2015). POSIT: Flexible shape-guided docking for pose prediction. *Journal of Chemical Information and Modeling*, 55(8), 1771–1780. <https://doi.org/10.1021/acs.jcim.5b00142>
- Kim, J., Jeong, S., Sarawut, S., Kim, H., Son, S. U., Lee, S., Rabbani, G., Kwon, H., Lim, E.-K., Ahn, S. N., & Park, S.-H. K. (2022). An immunosensor based on a high performance dual-gate oxide semiconductor thin-film transistor for rapid detection of SARS-CoV-2. *Lab on a Chip*, 22(5), 899–907. <https://doi.org/10.1039/d1lc01116b>
- Knipe, D. M. (2013). *Fields virology*. Lippincott Williams & Wilkins.
- Kollman, P. A., Massova, I., Reyes, C., Kuhn, B., Huo, S., Chong, L., Lee, M., Lee, T., Duan, Y., Wang, W., Donini, O., Cieplak, P., Srinivasan, J., Case, D. A., & Cheatham, T. E. (2000). Calculating structures and free energies of complex molecules: Combining molecular mechanics and continuum models. *Accounts of Chemical Research*, 33(12), 889–897. <https://doi.org/10.1021/ar000033j>
- Li, F. (2015). Receptor recognition mechanisms of coronaviruses: A decade of structural studies. *Journal of Virology*, 89(4), 1954–1964. <https://doi.org/10.1128/JVI.02615-14>

- Li, F. (2016). Structure, function, and evolution of coronavirus spike proteins. *Annual Review of Virology*, 3(1), 237–261. <https://doi.org/10.1146/annurev-virology-110615-042301>
- Li, W., Chen, Y., Prévost, J., Ullah, I., Lu, M., Gong, S. Y., Tazuin, A., Gasser, R., Vézina, D., Anand, S. P., Goyette, G., Chatterjee, D., Ding, S., Tolbert, W. D., Grunst, M. W., Bo, Y., Zhang, S., Richard, J., Zhou, F., ... Mothes, W. (2022). Structural basis and mode of action for two broadly neutralizing antibodies against SARS-CoV-2 emerging variants of concern. *Cell Rep*, 38(2), 110210. <https://doi.org/10.1016/j.celrep.2021.110210>
- Liu, C., Ginn, H. M., Dejnirattisai, W., Supasa, P., Wang, B., Tuekprakhon, A., Nutalai, R., Zhou, D., Mentzer, A. J., Zhao, Y., Duyvesteyn, H. M., López-Camacho, C., Slon-Campos, J., Walter, T. S., Skelly, D., Johnson, S. A., Ritter, T. G., Mason, C., Costa Clemens, S. A., ... Sreaton, G. R. (2021). Reduced neutralization of SARS-CoV-2 B. 1.617 by vaccine and convalescent serum. *Cell*, 184(16), 4220–4236. <https://doi.org/10.1016/j.cell.2021.06.020>
- Lu, G., Wang, Q., & Gao, G. F. (2015). Bat-to-human: Spike features determining 'host jump' of coronaviruses SARS-CoV, MERS-CoV, and beyond. *Trends in Microbiology*, 23(8), 468–478. <https://doi.org/10.1016/j.tim.2015.06.003>
- Maier, J. A., Martinez, C., Kasavajhala, K., Wickstrom, L., Hauser, K. E., & Simmerling, C. (2015). ff14SB: Improving the accuracy of protein side chain and backbone parameters from ff99SB. *Journal of Chemical Theory and Computation*, 11(8), 3696–3713. <https://doi.org/10.1021/acs.jctc.5b00255>
- McGann, M. (2011). FRED pose prediction and virtual screening accuracy. *Journal of Chemical Information and Modeling*, 51(3), 578–596. <https://doi.org/10.1021/ci100436p>
- McGann, M. (2012). FRED and HYBRID docking performance on standardized datasets. *Journal of Computer-Aided Molecular Design*, 26(8), 897–906. <https://doi.org/10.1007/s10822-012-9584-8>
- Miller, B. R., III, McGee, T. D., Jr., Swails, J. M., Homeyer, N., Gohlke, H., & Roitberg, A. E. (2012). MMPBSA.py: An efficient program for end-state free energy calculations. *Journal of Chemical Theory and Computation*, 8(9), 3314–3321. <https://doi.org/10.1021/ct300418h>
- Molchanova, N., Hansen, P. R., & Franzyk, H. (2017). Advances in development of antimicrobial peptidomimetics as potential drugs. *Molecules*, 22(9), 1430. <https://doi.org/10.3390/molecules22091430>
- Narkhede, R. R., Cheke, R. S., Ambhore, J. P., & Shinde, S. D. (2020). The molecular docking study of potential drug candidates showing anti-COVID-19 activity by exploring of therapeutic targets of SARS-CoV-2. *Eurasian Journal of Medicine and Oncology*, 4(3), 185–195.
- Pandey, P., Rane, J. S., Chatterjee, A., Kumar, A., Khan, R., Prakash, A., & Ray, S. (2021). Targeting SARS-CoV-2 spike protein of COVID-19 with naturally occurring phytochemicals: An in silico study for drug development. *Journal of Biomolecular Structure & Dynamics*, 39(16), 6306–6316. <https://doi.org/10.1080/07391102.2020.1796811>
- Patrick, G. L. (Ed.). (2020). Plasmepsins as targets for antimalarial agents. In *Antimalarial agents* (pp. 217–270). Elsevier.
- Polack, F. P., Thomas, S. J., Kitchin, N., Absalon, J., Gurtman, A., Lockhart, S., Perez, J. L., Pérez Marc, G., Moreira, E. D., Zerbini, C., Bailey, R., Swanson, K. A., Roychoudhury, S., Koury, K., Li, P., Kalina, W. V., Cooper, D., Frenck, R. W., Hammitt, L. L., ... Gruber, W. C. (2020). Safety and efficacy of the BNT162b2 mRNA Covid-19 vaccine. *New England Journal of Medicine*, 383(27), 2603–2615. <https://doi.org/10.1056/NEJMoa2034577>
- Quimque, M. T. J., Notarte, K. I. R., Fernandez, R. A. T., Mendoza, M. A. O., Liman, R. A. D., Lim, J. A. K., Pilapil, L. A. E., Ong, J. K. H., Pastrana, A. M., Khan, A., Wei, D.-Q., & Macabeo, A. P. G. (2021). Virtual screening-driven drug discovery of SARS-CoV2 enzyme inhibitors targeting viral attachment, replication, post-translational modification and host immunity evasion infection mechanisms. *Journal of Biomolecular Structure & Dynamics*, 39(12), 4316–4333. <https://doi.org/10.1080/07391102.2020.1776639>
- Rabbani, G., & Ahn, S. N. (2021). Roles of human serum albumin in prediction, diagnoses and treatment of COVID-19. *International Journal of Biological Macromolecules*, 193(Pt A), 948–955. <https://doi.org/10.1016/j.ijbiomac.2021.10.095>
- Rabbani, G., Ahn, S. N., Kwon, H., Ahmad, K., & Choi, I. (2021). Penta-peptide ATN-161 based neutralization mechanism of SARS-CoV-2 spike protein. *Biochemistry and Biophysics Reports*, 28, 101170.
- Sachdeva, S., Joo, H., Tsai, J., Jasti, B., & Li, X. (2019). A rational approach for creating peptides mimicking antibody binding. *Scientific Reports*, 9(1), 1–11. <https://doi.org/10.1038/s41598-018-37201-6>
- Sharma, A., Tiwari, V., & Sowdhamini, R. (2020). Computational search for potential COVID-19 drugs from FDA-approved drugs and small molecules of natural origin identifies several anti-virals and plant products. *Journal of Biosciences*, 45(1), 1–18. <https://doi.org/10.1007/s12038-020-00069-8>
- Stierand, K., Maass, P. C., & Rarey, M. (2006). Molecular complexes at a glance: Automated generation of two-dimensional complex diagrams. *Bioinformatics (Oxford, England)*, 22(14), 1710–1716. <https://doi.org/10.1093/bioinformatics/btl150>
- Su, S., Wong, G., Shi, W., Liu, J., Lai, A. C. K., Zhou, J., Liu, W., Bi, Y., & Gao, G. F. (2016). Epidemiology, genetic recombination, and pathogenesis of coronaviruses. *Trends in Microbiology*, 24(6), 490–502. <https://doi.org/10.1016/j.tim.2016.03.003>
- Vagner, J., Qu, H., & Hruby, V. J. (2008). Peptidomimetics, a synthetic tool of drug discovery. *Current Opinion in Chemical Biology*, 12(3), 292–296. <https://doi.org/10.1016/j.cbpa.2008.03.009>
- Vanqualef, E., Simon, S., Marquant, G., Garcia, E., Klimerak, G., Delepine, J. C., Cieplak, P., & Dupradeau, F.-Y. (2011). RED Server: A web service for deriving RESP and ESP charges and building force field libraries for new molecules and molecular fragments. *Nucleic Acids Research*, 39(Web Server issue), W511–W517. <https://doi.org/10.1093/nar/gkr288>
- Voysey, M., Clemens, S. A. C., Madhi, S. A., Weckx, L. Y., Folegatti, P. M., Aley, P. K., Angus, B., Baillie, V. L., Barnabas, S. L., Bhorat, Q. E., Bibi, S., Briner, C., Cicconi, P., Collins, A. M., Colin-Jones, R., Cutland, C. L., Darton, T. C., Dheda, K., Duncan, C. J. A., ... Zuidewind, P. (2021). Safety and efficacy of the ChAdOx1 nCoV-19 vaccine (AZD1222) against SARS-CoV-2: An interim analysis of four randomised controlled trials in Brazil, South Africa, and the UK. *The Lancet*, 397(10269), 99–111. [https://doi.org/10.1016/S0140-6736\(20\)32661-1](https://doi.org/10.1016/S0140-6736(20)32661-1)
- Walls, A. C., Park, Y.-J., Tortorici, M. A., Wall, A., McGuire, A. T., & Velesler, D. (2020). Structure, function, and antigenicity of the SARS-CoV-2 spike glycoprotein. *Cell*, 181(2), 281–292. <https://doi.org/10.1016/j.cell.2020.02.058>
- Wang, J., Wang, W., Kollman, P. A., & Case, D. A. (2001). Antechamber: An accessory software package for molecular mechanical calculations. *Journal of the American Chemical Society*, 222, U403.
- Wang, J., Wang, W., Kollman, P. A., & Case, D. A. (2006). Automatic atom type and bond type perception in molecular mechanical calculations. *Journal of Molecular Graphics & Modelling*, 25(2), 247–260. <https://doi.org/10.1016/j.jmgm.2005.12.005>
- Wu, Y. (2020). A noncompeting pair of human neutralizing antibodies block COVID-19 virus binding to its receptor ACE2. *Science (1979)*, 368(6496), 1274–1278.
- Zamzami, M. A., Rabbani, G., Ahmad, A., Basalah, A. A., Al-Sabban, W. H., Nate Ahn, S., & Choudhry, H. (2022). Carbon nanotube field-effect transistor (CNT-FET)-based biosensor for rapid detection of SARS-CoV-2 (COVID-19) surface spike protein S1. *Bioelectrochemistry*, 143, 107982. <https://doi.org/10.1016/j.bioelechem.2021.107982>
- Zhou, D., Dejnirattisai, W., Supasa, P., Liu, C., Mentzer, A. J., Ginn, H. M., Zhao, Y., Duyvesteyn, H. M., Tuekprakhon, A., Nutalai, R., Wang, B., Paesen, G. C., Lopez-Camacho, C., Slon-Campos, J., Hallis, B., Coombes, N., Bewley, K., Charlton, S., Walter, T. S., ... Sreaton, G. R. (2021). Evidence of escape of SARS-CoV-2 variant B. 1.351 from natural and vaccine-induced sera. *Cell*, 184(9), 2348–2361. <https://doi.org/10.1016/j.cell.2021.02.037>
- Zhou, D., Duyvesteyn, H. M. E., Chen, C.-P., Huang, C.-G., Chen, T.-H., Shih, S.-R., Lin, Y.-C., Cheng, C.-Y., Cheng, S.-H., Huang, Y.-C., Lin, T.-Y., Ma, C., Huo, J., Carrique, L., Malinauskas, T., Ruza, R. R., Shah, P. N. M., Tan, T. K., Rijal, P., ... Huang, K.-Y. A. (2020). Structural basis for the neutralization of SARS-CoV-2 by an antibody from a convalescent patient. *Nature Structural & Molecular Biology*, 27(10), 950–958. <https://doi.org/10.1038/s41594-020-0480-y>
- Zhu, N., Zhang, D., Wang, W., Li, X., Yang, B., Song, J., Zhao, X., Huang, B., Shi, W., Lu, R., Niu, P., Zhan, F., Ma, X., Wang, D., Xu, W., Wu, G., Gao, G. F., & Tan, W. (2020). A novel coronavirus from patients with pneumonia in China, 2019. *New England Journal of Medicine*, 382(8), 727–733. <https://doi.org/10.1056/NEJMoa2001017>